On the Validity of the Boltzmann-BGK Model

Quanhua Sun*, Wei Gao

State Key Laborotary of High Temperature Gas Dynamics, Institute of Mechanics, CAS
No. 15, Beisihuanxi Road, Beijing, 100190, China

Abstract

The Boltzmann-BGK model is investigated for its validity on the collision term approximation through relaxation evaluation. The evaluation is based on theoretical analysis and numerical comparison between BGK and DSMC results for three designed relaxation problems. In order to isolate model-induced error, the BGK results are derived theoretically whereas numerical error in DSMC results is well controlled. It is analyzed that the relaxation time in BGK model does not equal to molecular mean collision time. Relaxation of 1D-space distribution fails to involve enough contribution from distributions in other dimensions, which makes the BGK model unable to capture details of velocity distribution, especially when discontinuity exists in distribution. The BGK model, however, predicts satisfactory history of velocity distribution function during relaxation when the flow is not far from Maxwellian. Particularly, the model-induced error in BGK depends on the degree of nonequilibirum, thus the model is more applicable for low-speed flows than for hypersonic flows. Because relaxation problem has no direct connection to Knudsen number, the BGK model can be applied to high rarefied flow as long as degree of nonequilibrium is not strong.

Keywords: Boltzmann equation; BGK model; DSMC method; velocity distribution function; time relaxation

1. Introduction

The Boltzmann equation describes the fundamental and general microscopic behavior of a dilute gas, which forms the basis of the kinetic theory of gases [1]. The nonlinear multidimensional integral collision term in the equation makes the full Boltzmann equation difficult to be solved. Thus, simple expressions have been proposed to replace the collision integral [2-6], and the resulted equation is called a model equation or kinetic model. A kinetic model enables the macroscopic laws to be derived from elementary principles and allows to deduce transport coefficients, which has arose renewed interests in the solution of model equations in recent years [7-11].

The most popular and widely used kinetic model is the Bhatnagar-Gross-Krook (BGK) model in which the collision term is replaced with a simple relaxation expression [2]. It is assumed that the net effect of collisions makes the velocity distribution function relax toward a local equilibrium distribution over a characteristic time. This treatment greatly simplifies the Boltzmann equation but produces an inaccurate Prandtl number (it is unity rather than 2/3 for monatomic gases). To fix the Prandtl number in the BGK model, many modified models have been proposed. These include the ellipsoidal-statistical (ES) BGK model [3] and the Shakhov model [4].

However, it is hard to validate the BGK-type model theoretically. Studies have been focused on numerical evaluation on test problems. For instance, Kumar et al. [12] assessed the BGK approaches for near continuum nozzle flows, and the solutions of the BGK equations were found to be in good agreement with the direct simulation Monte Carlo (DSMC) results. Andries et al. [13] showed that the ES-BGK solutions agreed well with the DSMC results for planar Couette flow and for supersonic flow over a flat plate when the Knudsen (Kn) number is less than 0.01. For large Knudsen number flows, however, the accuracy of BGK models was found to be poor. Mieussens and Struchtrup [14] compared several BGK-type models for Couette flow and stationary

* Corresponding author: qsun@imech.ac.cn

shock wave problems. They concluded that all BGK models with proper Prandtl number were accurate in the continuum regime, qualitatively good in the transitional regime and inaccurate at large Knudsen numbers and for shock structures. This observation can be applied to nearly all test problems in the literature until recently Xu et al. developed a unified gas-kinetic scheme [15] and showed that the unified scheme was a reliable and accurate solver for low speed non-equilibrium flows [16]. Their observation seems to be inconsistent with previous findings.

Up to now, BGK models have been evaluated using specific test problems with different numerical schemes. Because schemes will more or less cause numerical error when the model equation is solved, it is hard to tell whether any error in a numerical solution comes from the approximation of the BGK model or from the numerical scheme or from both. In this paper, validity of BGK model will be evaluated by comparing its exact solution to Boltzmann result for several designed relaxation problems. Detailed evaluation will pay attention to velocity distribution function, macroscopic properties, and fluxes. Effects of nonequilibrium strength on model validity will also be investigated.

2. Theoretical analysis

2.1. BGK model

The BGK model [2] is a kinetic model proposed by Bhatnagar, Gross, and Krook as an approximation to the Boltzmann equation:

$$\frac{\partial f}{\partial t}+\mathbf{V}\cdot\frac{\partial f}{\partial \mathbf{r}}+\frac{\mathbf{F}}{m}\cdot\frac{\partial f}{\partial \mathbf{V}}=\nu\left(f_M-f\right), \tag{1}$$

where f is the molecular velocity distribution function, a function of time t, position $\mathbf{r}$ and velocity $\mathbf{V}$. $\mathbf{F}$ is the external force. The right hand side is the collision term, which is modeled as a relaxation process with an equilibrium distribution f_M and a relaxation rate ν. This expression is much simpler than its Boltzmann counterpart:

$$\left[\frac{\partial f}{\partial t}\right]_{coll}=\int_{-\infty}^{\infty}\int_{0}^{4\pi}\left(f^{*}f_1^{*}-ff_1\right)\left|\mathbf{v}-\mathbf{v}_1\right|\sigma d\Omega d\mathbf{v}_1 . \tag{2}$$

Here, distribution function f and f^* are evaluated at molecule's pre-collision velocity $\mathbf{v}$ and post-collision velocity $\mathbf{v}^*$, whereas f_1 and f_1^* are evaluated at collision partner's pre-collision velocity $\mathbf{v_1}$ and post-collision velocity $\mathbf{v_1}^*$, respectively. In addition, σ is the collision cross section of collision pair and Ω is the solid angle.

It is well known that the collision term approximation is accurate when the relaxation rate is infinite or zero because the collision term vanishes in both cases. For general flow description, the BGK model is approximate since details of two-body interactions are ignored in the collision term. The relaxation rate is determined as $\nu=\frac{p}{\mu}$ in order to satisfy the Navier-Stokes equation when it is derived from the BGK model using the Chapman-Enskog expansion [17]. However, the BGK model has only one free parameter, it is impossible to simulate all physical properties such as thermal conductivity and self-diffusion. Therefore, additional parameters are required for extended BGK models to simulate correctly the other physical properties of a gas flow. For instance, the ES-BGK model includes a Prandtl number as a free parameter to capture the heat flux.

It should be noticed that the relaxation rate in the BGK model is not the same as the collision rate. The collision rate can be evaluated using kinetic theory [11, 18]. It is velocity independent for Maxwell molecule ($\mu\propto T$) and has the general expression,

$$\nu_c=\frac{(\alpha+1)(\alpha+2)}{3\alpha}\frac{p}{\mu} \tag{3}$$

where α is the angular scattering exponent. For isotropic scattering (α=1.0), $\nu_c = 2\nu$. For monatomic gas (α=2.14), $\nu_c \approx 2\nu$. Clearly, the collision rate is generally larger than the relaxation rate although molecular model will slightly affect the value of the collision rate.

It is interesting to note that Vincenti and Kruger [11] related vf to the depleting term $f f_1$ and vf_M to the replenishing term $f^* f_1^*$ by comparing the physical form of the BGK and Boltzmann collision terms. They argued that the assumption for the replenishing term to be equal to vf_M could be considered equivalent to this approximation: the molecules after a collision were instantaneously accommodated to a local Maxwellian distribution. Since a pair of collide particles are not aware of the local macroscopic temperature, such approximation is questionable. In fact, the depleting term in the Boltzmann equation can be easily evaluated for Maxwell molecules ($\sigma \propto |\mathbf{v}-\mathbf{v}_1|^{-1}$):

$$\int_{-\infty}^{\infty}\int_{0}^{4\pi} ff_1 |\mathbf{v}-\mathbf{v}_1| \sigma d\Omega d\mathbf{v}_1 = \nu_c f \tag{4}$$

This means that the depleting term $f f_1$ corresponds to $\nu_c f$ instead of vf. Then the replenishing term $f^* f_1^*$ corresponds to $(\nu_c - \nu) f + \nu f_M$ if the BGK model is followed. Namely, the replenishing term $f^* f_1^*$ corresponds to $\nu_c \dfrac{f_M + f}{2}$. This approximation of the replenishing term indicates that molecules after a collision are accommodated to the average of own pre-collision and local equilibrium distribution instead of fully local Maxwellian distribution. This sounds more reasonable than the original interpretation [17].

However, it is difficult to establish a precise relationship between the Boltzmann collision integral and BGK collision model. Theoretical validation of BGK models is usually performed in the frame of the Navier-Stokes equation. General requirements are the conservation law, H-theorem, correct viscosity and thermal conductivity, and positive distribution. These requirements, however, cannot cover features of the Boltzmann collision integral in the entire flow regime. Although BGK models have the potential to predict correct values for macroscopic quantities, they may not produce exact microscopic velocity distribution.

2.2. Relaxation solution

BGK models replace the Boltzmann collision term with a simple relaxation expression. This relaxation expression then determines the validity of BGK model. Analyzing the relaxation process of the distribution function is probably the best approach to validate the model.

The relaxation process in the BGK model is governed by

$$\frac{\partial f}{\partial t} = \nu (f_M - f), \tag{5}$$

where the convection and acceleration terms are neglected. This equation can be integrated explicitly [19]:

$$f(t) = g + e^{-\nu t}(f(0) - g), \tag{6}$$

where $g=f_M$ is the Maxwellian distribution. Thus given the initial condition of distribution, its time evolution can be exactly calculated for the BGK equation.

With the velocity distribution function, it is convenient to calculate moments of the distribution. Particular, the component velocity distribution function can be derived from Eq (6) by integrating the other two velocity spaces. For instance,

$$f_x(t) = \int_{-\infty}^{\infty}\int_{-\infty}^{\infty} f dV_y dV_z = g_x + e^{-\nu t}(f_x(0) - g_x). \tag{7}$$

This expression shows that the x-component velocity distribution depends only on the initial and final x-component velocity distribution as the time goes. Clearly, details of the other components have no impact on the x-component velocity distribution other than effects through the equilibrium distribution. This obviously

causes error because many different initial distributions can lead to a same equilibrium distribution. The error is difficult to be quantified theoretically, however. An alternative way is to compare numerical solutions of BGK model and Boltzmann equation.

2.3. DSMC method

Although the Boltzmann equation is difficult to solve, numerical solution of the Boltzmann equation can be easily obtained for the relaxation problem using the direct simulation Monte Carlo (DSMC) method [18].

The DSMC method is a particle simulation approach that tracks the motion and collisions of microscopic molecules. It follows the statistical physics of binary collisions and assumes that motion and collisions can be decoupled during a very short time. The solution obtained using the DSMC method has been proved by Wagner [20] to be consistent to the solution of the Boltzmann equation for a monatomic gas.

A valid DSMC simulation has strict computational requirement because its numerical error mainly comes from the time step, cell size, number of particles per cell, and the sample size. For instance, Rader et al. [21] showed that the numerical error in thermal conductivity for Fourier heat flow of hard sphere gas was about $0.0405\left(\Delta x/\lambda\right)^2$ due to the cell size, $0.0287\left(\Delta t/\tau\right)^2$ due to the time step, and $0.083/N_c$ due to the number of particles per cell, where λ is the mean free path and τ is the mean collision time. The statistical error due to a limited sample size is proportional to $1/\sqrt{N_s}$ for flow properties such as velocity, density, and temperature [22], where N_s can be enlarged using ensemble average.

In this paper, the standard DSMC algorithm is implemented [18]. For instance, the no-time-counter (NTC) method is used to select particles for collisions. Because the relaxation rate in the BGK model is independent on the molecular velocity, the Maxwell molecular model is employed for DSMC simulations. In addition, DSMC simulations use isotropic scattering for post-collisions as the BGK model has no specification for self-diffusion. For relaxation problems, simulated gas is argon. Its molecular diameter is 4.59×10^{-10}m at 273K to match the viscosity of 2.117×10^{-5}Ns/m^2. The time step is fixed at 0.01τ and totally 8,000,000 particles are simulated. With this specification, the numerical error from a DSMC simulation is negligible, and obtained DSMC results can be treated as Boltzmann solution.

3. Numerical comparison of nonequilibrium relaxation

In order to illustrate the validity of the BGK model, three kinds of relaxation problems are designed. The first is an anisotropic Maxwellian distribution. Specifically, the distribution for each velocity component is Maxwellian, but has different temperature value. The second is double half-normal distribution. That is, a full distribution is comprised of two half-normal distributions in one velocity space, and distributions in the other velocity spaces are Maxwellian. This test is used to show the development of discontinuity in the distribution. The third is a tailored half-Maxwellian distribution. This is similar to the second case except that the discontinuity is removed by adjusting the amplitude of half distributions. It is a rather general case that the distribution is continuous and asymmetric.

For the sake of easy comparison, the default Maxwellian distribution is specified at a temperature of 273K and a mean velocity of zero. The initial difference for relaxation is realized by setting one-component or half Maxwellian distribution using a temperature other than 273K. The strength of nonequilibrium degree depends on the temperature difference. For this purpose, four values (373K, 546K, 1365K, and 2730K) are used for the other temperature.

3.1. Relaxation of anisotropic Maxwellian distribution

The anisotropic Maxwellian distribution is specified as follows:

$$f(0)=\frac{\beta_1}{\sqrt{\pi}}\exp\left(-\beta_1^2u^2\right)\frac{\beta_2}{\sqrt{\pi}}\exp\left(-\beta_2^2v^2\right)\frac{\beta_2}{\sqrt{\pi}}\exp\left(-\beta_2^2w^2\right), \tag{8}$$

where $\beta_i=\sqrt{\frac{m}{2kT_i}}$. The macroscopic temperature is the average of component temperatures, which is constant during the relaxation.

Figure 1 shows the x-component velocity distribution functions at several time moments where the BGK solution and DSMC results are compared. During the relaxation process, the maximum probability density increases and the distribution width decreases with the time, because the initial temperature T_1 is larger than 273K. It seems that an equilibrium state is nearly reached at t=5τ. In general, the agreement between BGK and DSMC results is satisfactory during the entire relaxation process. Slight difference, however, is observed when T_1 is increased from 546K to higher values during the nonequilibrium stage. Particularly, the BGK model overpredicts the maximum probability density, and the error is proportional to the inital temperature difference.

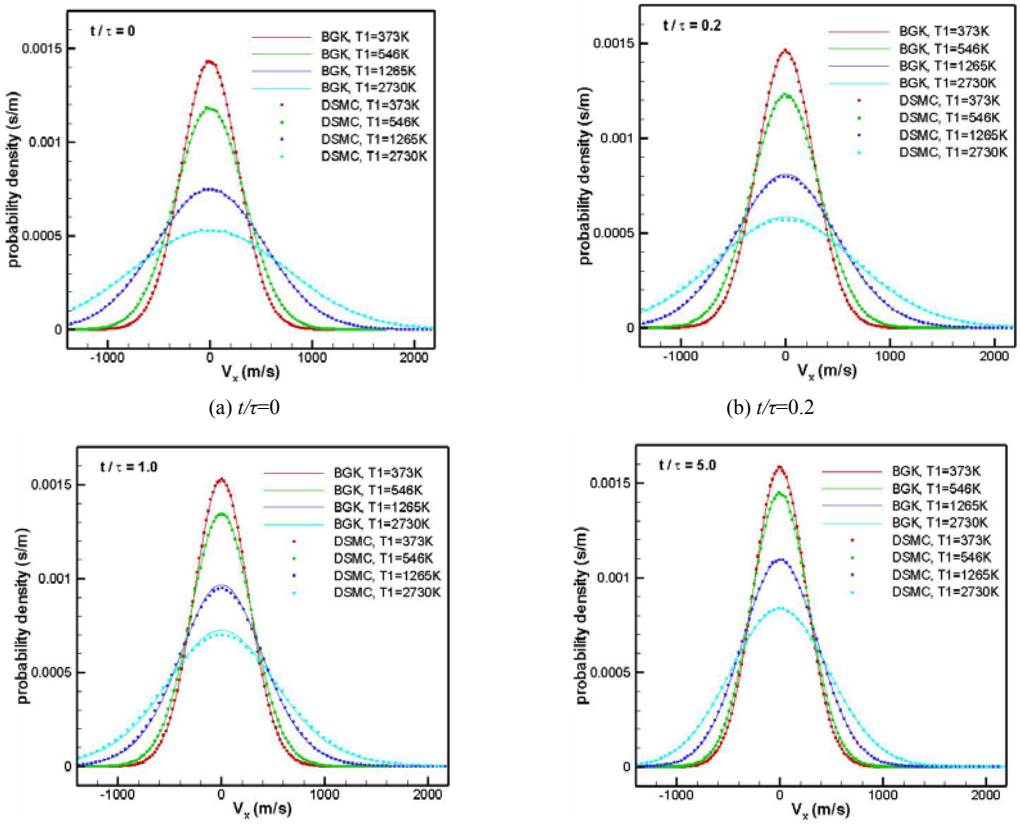

(a) t/τ=0 (b) t/τ=0.2

(c) t/τ=1.0 (d) t/τ=5.0

Fig. 1 Comparison of x-component velocity distributions during relaxation of anisotropic Maxwellian distribution when T_2= 273K and T_1=373K, 546K, 1365K, or 2730K. Solid lines are exact BGK solution and symbols represent DSMC results.

3.2. Relaxation of double half-normal distribution

The double half-normal distribution is designed as:

$$f(0)=\left(\frac{\beta_1}{\sqrt{\pi}}\exp\left(-\beta_1^2u^2\right)\Big|_{u<0}+\frac{\beta_2}{\sqrt{\pi}}\exp\left(-\beta_2^2u^2\right)\Big|_{u\geq 0}\right)\frac{\beta_2}{\sqrt{\pi}}\exp\left(-\beta_2^2v^2\right)\frac{\beta_2}{\sqrt{\pi}}\exp\left(-\beta_2^2w^2\right) \tag{9}$$

Here the x-component distribution is comprised of two half-normal distributions. This is a distribution having a discontinuity in the velocity space. Similar discontinuity can be found in collisionless flow between two parallel plates with different temperatures and collisionless jet impingement problems [23]. It can be derived that the x-component mean velocity is

$$U = \sqrt{\frac{k}{2\pi m}}\left(\sqrt{T_2} - \sqrt{T_1}\right), \tag{10}$$

and the macroscopic temperature is

$$T = \frac{1}{3}\left(\frac{T_1 + T_2}{2}\left(1 - \frac{1}{\pi}\right) + \frac{\sqrt{T_1 T_2}}{\pi} + 2T_2\right) \tag{11}$$

Figure 2 shows the probability density for the x-component velocity at several time moments. Again, the DSMC and BGK results are plotted for four values of initial temperature T_1. Because of initial discontinuity, the probability density shows different profile on the two sides. When V_x>0, the BGK results generally agree with DSMC results except some difference near the discontinuity. When V_x<0, however, there is significant difference during the relaxation process. For instance, when t=1.0τ, the probability density monotonically increases with the velocity in the DSMC results whereas the BGK profile depends on the initial temperature. When T_1=373K, the BGK result agrees well with the DSMC result. But when T_1=1365K or 2730K, the BGK profile has a strong decrease near the discontinuity. This behavior of BGK results is not surprising as the relaxation in BGK follows Eq (7).

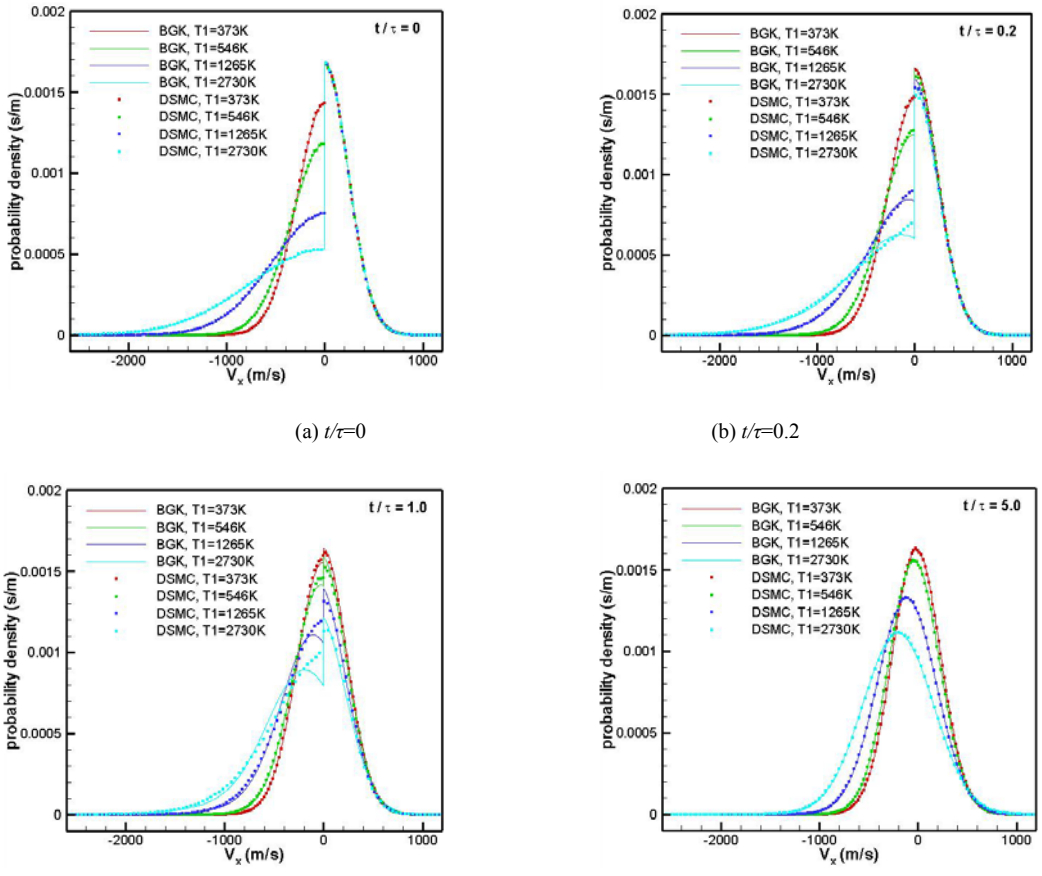

(a) t/τ=0 (b) t/τ=0.2

(c) t/τ=1.0 (d) t/τ=5.0

Fig. 2 Comparison of x-component velocity distributions during relaxation of double half-normal distribution when T_2= 273K and T_1=373K, 546K, 1365K, or 2730K. Solid lines are exact BGK solution and symbols represent DSMC results.

Figure 3 illustrates the evaluation of BGK results at t=1.0τ. Using Eq (7), the instantaneous distribution (solid cyan line) from BGK model is the combination of the initial (dashed red line) and final (dash-dot blue line) distributions. The local minimum near the discontinuity in BGK solution is actually unreasonable. The DSMC results (black symbol) show that the y- and z-component distributions (dashed green line) have obvious contribution to the x-component, which indicates the failure of BGK in this aspect.

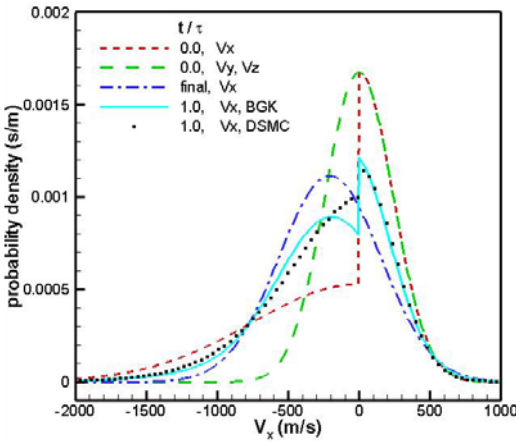

Fig. 3 Comparison of velocity distributions between BGK and DSMC results when t=1.0τ with initial component distributions and final equilibrium distribution for the double-half distribution case.

3.3. Relaxation of tailored half-Maxwellian distribution

The tailored half-Maxwellian distribution is designed as follows:

$$f(0)=\frac{2}{\sqrt{\pi}}\frac{\beta_1\beta_2}{\beta_1+\beta_2}\left(\exp\left(-\beta_1^2u^2\right)\Big|_{u<0}+\exp\left(-\beta_2^2u^2\right)\Big|_{u\geq 0}\right)\frac{\beta_2}{\sqrt{\pi}}\exp\left(-\beta_2^2v^2\right)\frac{\beta_2}{\sqrt{\pi}}\exp\left(-\beta_2^2w^2\right) \tag{12}$$

This is a smooth distribution for the x-component velocity but the semi-width of each half is different. The x-component mean velocity is

$$U=\sqrt{\frac{2k}{\pi m}}\left(\sqrt{T_2}-\sqrt{T_1}\right), \tag{13}$$

and the macroscopic temperature is

$$T=\frac{1}{3}\left(\left(1-\frac{2}{\pi}\right)(T_1+T_2)+\left(\frac{4}{\pi}-1\right)\sqrt{T_1T_2}+2T_2\right) \tag{14}$$

Figure 4 shows the probability density for the x-component velocity at several time moments. Clearly, the initial distribution is asymmetric, especially when T1 is larger than 1000K. The general agreement between BGK and DSMC results is satisfactory during the entire relaxation process. However, slight difference is observed during the nonequilibrium state, which is similar to the anisotropic case. In addition, this difference increases with the initial temperature disparity.

3.4. Discussions

Since the BGK model is an approximate model, it is not surprising to have error in the velocity distribution function. The current comparison between BGK and DSMC results, however, shows that the BGK model predicts unexpected good relaxation history for the anisotropic distribution and tailored half-Maxwellian distribution cases. In fact, the model-induced error is negligible when the difference in initial distribution is small (say $T_1<2T_2$), and the error increases when the initial difference is enlarged. For the double half-normal distribution case, the model-induced error is relatively large because there is discontinuity in the initial

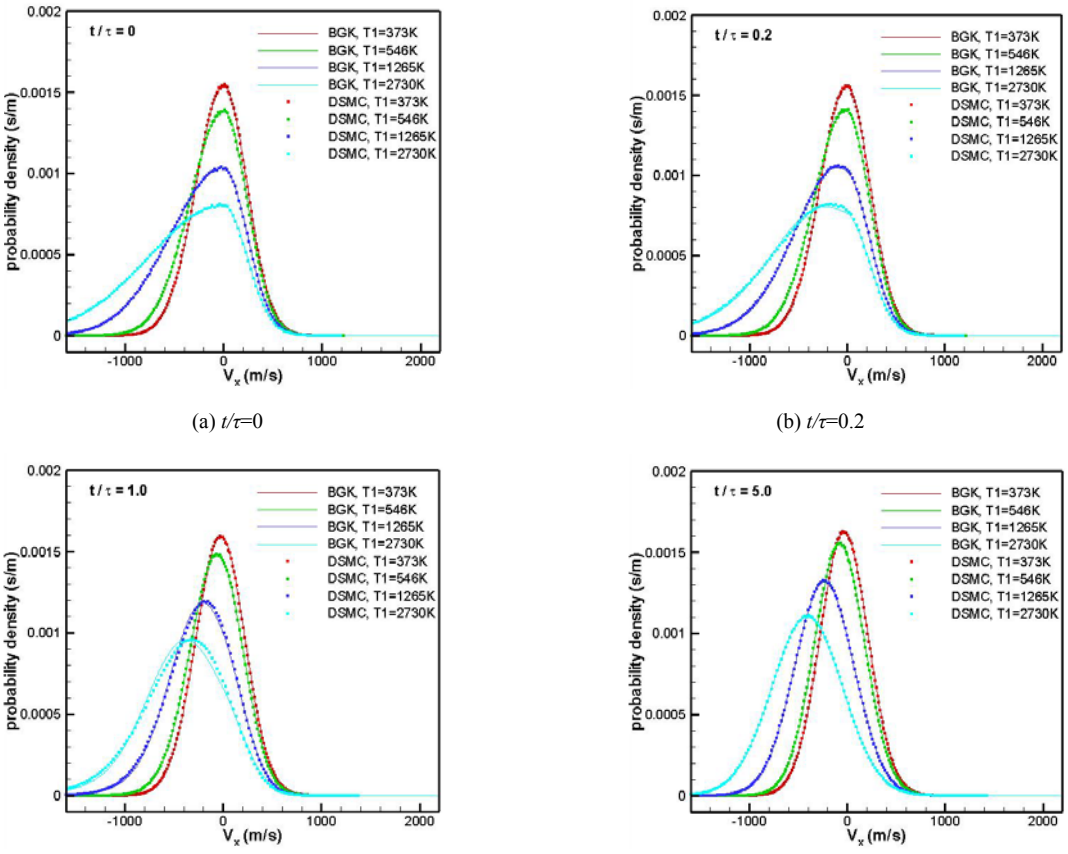

(a) t/τ=0 (b) t/τ=0.2

(c) t/τ=1.0 (d) t/τ=5.0

Fig. 4 Comparison of x-component velocity distributions during relaxation of tailored half-Maxwellian distribution when T_2= 273K and T_1=373K, 546K, 1365K, or 2730K. Solid lines are exact BGK solution and symbols represent DSMC results.

distribution. The general behavior of model-induced error for this case is the same as the other two cases. Based on this fact, it is reasonable to argue that the BGK model works well for near-equilibrium distributions and shows a model-induced error that increases with the degree of nonequilibrium. That means, the BGK model can work well for low speed flows even when the flow Knudsen number is larger than 1, and it may fail to predict hypersonic flow even when Kn is less than 0.1, because the distribution function departures from local Maxwellian more for hypersonic flow than for low-speed flow at same Knudsen number.

The current comparison focuses only on Maxwell molecular model. For other molecular model such as variable hard sphere (VHS) model, the BGK model needs only to adjust its relaxation rate. The model-induced error, however, displays the same general behavior although small disparity is observed in DSMC results when molecular model changes. Particularly, the scattering exponent in molecular collision model has little effect on the distribution function for current cases.

4. Validity analysis of BGK results

Comparison of velocity distribution function can provide overall difference between BGK and DSMC results. Since the shape of distributions can be quantified using central moments, it is useful to show the error in shape factors. In addition, macroscopic information may be more useful for engineering purpose. Therefore, distribution functions are integrated to make further comparison. The case of tailored half-Maxwellian distribution is employed to analyze the BGK validity because the general behavior is similar for all test cases.

4.1. Shape of the velocity distribution function

A velocity distribution function can be characterized by its central moments. Knowing the first few moments of the function gives a rough idea of the shape. The complete set of moments is equivalent to knowing the function. The central moments are defined as,

$$\overline{(u')^n} = \int_{-\infty}^{\infty} (u')^n f(u') du' \tag{15}$$

where $u' = u - \bar{u}$. Thus the first moment $\overline{(u')^1} = 0$. The second moment $\overline{(u')^2} = \sigma^2$ is called the variance of u and σ is called the standard deviation or the root mean square fluctuation value of u. This moment gives indication of the relative width of the distribution function. The third moment is usually expressed in the form of skewness $S = \overline{(u')^3} / \sigma^3$. Physically, S gives an indication of the degree of asymmetry for a distribution. The fourth moment is given in the form of kurtosis or flatness of the function $K = \overline{(u')^4} / \sigma^4$. K gives an indication of how much of the area is the tails of the distribution function. For a Maxwellian or Gaussian distribution, $\sigma = 1/\sqrt{2}\beta$ and is the half-width at the $e^{-0.5}$ (~0.607) point, S=0, and K=3.

For relaxation problems, explicit expressions can be derived for distribution moments in BGK (see appendix). Figure 5 shows the central moments (second, third, and fourth) of the velocity distribution as a function of time. Clearly, the agreement between BGK and DSMC results on the second central moment is satisfactory whereas the skewness and kurtosis show some disparity. It shows that the BGK distribution relaxes to symmetric state faster and has larger kurtosis than DSMC during the relaxation process. This disparity increases with the initial temperature difference. Namely, the disparity is negligible when T1=373K and becomes significant when T1>1000K. It is concluded that BGK model can predict precisely the second moment of the velocity distribution, but may not be the higher moments especially for strong nonequilibrium cases.

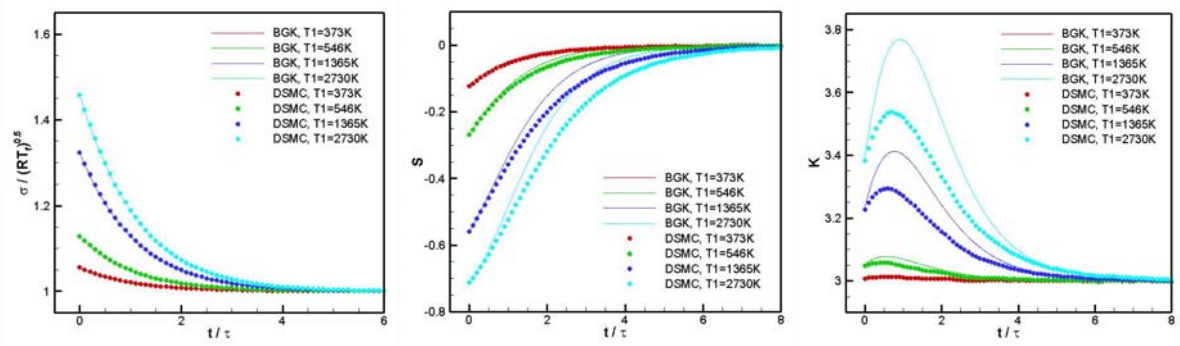

(a) second central moment (b) third central moment (c) fourth central moment

Fig. 5 Comparison of central moments (second, third, and fourth) of velocity distribution as a function of time between BGK and DSMC results for tailored half-Maxwellian distribution case.

4.2. Macroscopic temperature

During the relaxation process, mass, momentum and energy are conserved. The component temperature changes with time due to collisions. In the BGK model, the component temperature can be evaluated using Eq. (7) as follows:

$$T_i(t) = T + e^{-\nu t}\left(T_i(0) - T\right) \tag{16}$$

Figure 6 shows the history of component temperatures during the relaxation. Clearly, the agreement is excellent between the BGK and DSMC results regardless of the temperature difference.

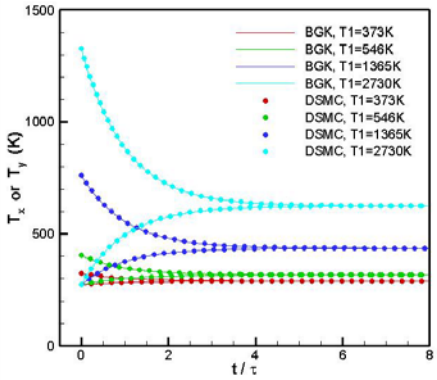

Fig. 6 Relaxation of T_x and T_y predicted using the BGK model and DSMC simulation for tailored half-Maxwellian distribution case.

4.3. Fluxes

For many numerical schemes in computational simulation, flux evaluation is critical to the accuracy of a simulation. For this reason, results of fluxes in the x direction are evaluated. In addition, half fluxes are compared between the BGK and DSMC results since this information is important for non-uniform flows.

Figure 7 shows the relaxation of x-component momentum and energy fluxes along the x direction. The mass flux is not plotted since it is time independent. It shows that momentum fluxes are well captured by the BGK model. The overall agreement on energy flux is also good except that the BGK relaxation is slightly faster. Unlike disparity in other comparisons, it seems that difference on the energy flux does not depend on initial temperature difference (or nonequilibrium degree). Because the BGK model predicts a larger Prandtl number (1>2/3), the fast relaxation behavior in BGK should not be the problem due to the Prandtl number issue. Figure 8 shows the relaxation of half fluxes along the positive x-direction. Unlike the full flux situation, there is disparity between BGK and DSMC for mass, momentum, and energy half fluxes. Again, this disparity depends on initial temperature difference.

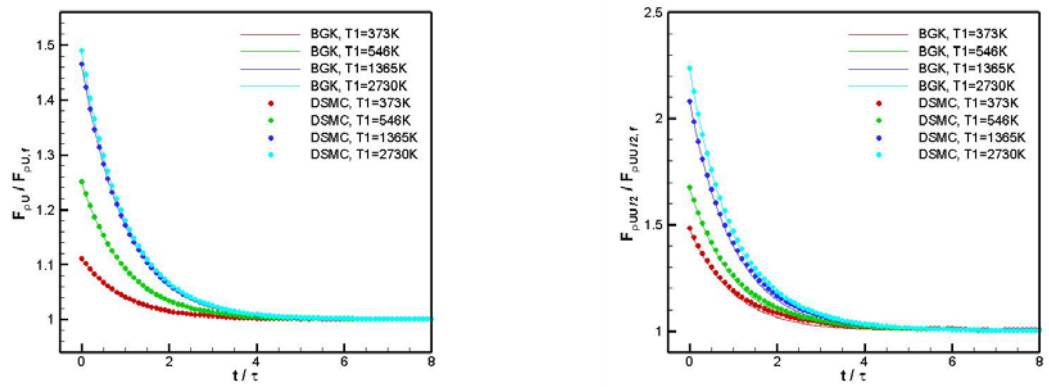

Fig. 7 Relaxation of momentum and energy fluxes in the x direction predicted using BGK model and DSMC simulation for tailored half-Maxwellian distribution case.

4.4. Discussions

This section has compared several integrations of velocity distribution function between BGK and DSMC. Among these integrals, the second central moment, the component temperature, and the moment flux, are all related to integration of second moments. Thus their behavior is the same and is well captured by the BGK model. The energy flux is nearly captured by BGK. Its error is relatively small and comes from the third

moments. This indicates that BGK has challenge to model correctly higher moments as shown in skewness and kurtosis.

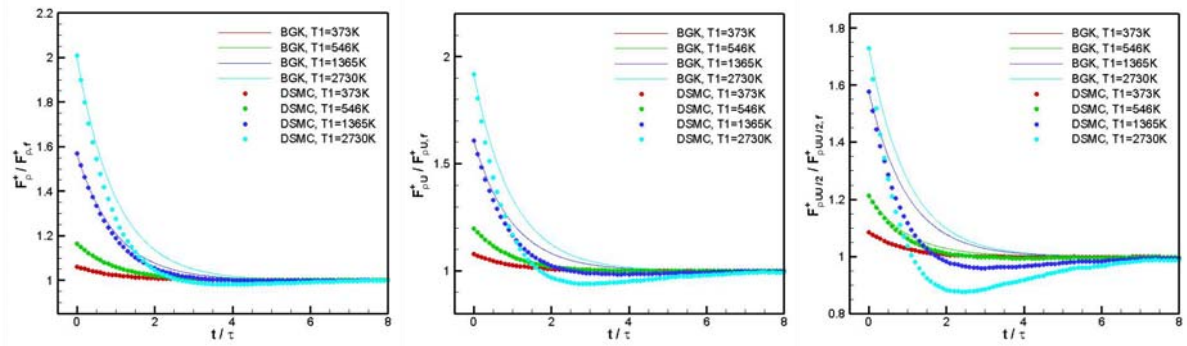

Fig. 8 Relaxation of half fluxes (mass, x-component momentum, energy) in the positive x direction predicted using BGK model and DSMC simulation for tailored half-Maxwellian distribution case.

4.5. Discussions

This section has compared several integrations of velocity distribution function between BGK and DSMC. Among these integrals, the second central moment, the component temperature, and the moment flux, are all related to integration of second moments. Thus their behavior is the same and is well captured by the BGK model. The energy flux is nearly captured by BGK. Its error is relatively small and comes from the third moments. This indicates that BGK has challenge to model correctly higher moments as shown in skewness and kurtosis.

The half flux evaluation is critical for application of the BGK model. It turns out that BGK results are good when degree of nonequilibrium (initial temperature difference) is weak and become worse for stronger nonequlibrium cases. Notice that velocity distribution function can be far from Maxwellian as within strong shock wave [18]. This indicates that the BGK model is more applicable for low-speed flows than for hypersonic flows.

5. Concluding remarks

In this paper, the validity of the BGK model has been analyzed and investigated using three relaxation problems. The BGK solution is accurate and numerical error in DSMC results is negligible. Difference between BGK and DSMC can be regarded as pure model-induced error in BGK.

The BGK model approximates the collision term in Boltzmann equation with a relaxation expression. The relaxation time is unequal to molecular mean collision time, thus the equilibrium part does not correspond to the replenishing part in the Boltzmann collision integral. For relaxation problems, distribution function in one-dimension only depends on its initial and final distribution in BGK, which ignores detailed information of distributions in other dimensions. This is the main reason why the BGK model cannot capture the details of the velocity distribution function.

However, the BGK model predicts satisfactory history of velocity distribution function during relaxation when the flow is not far from Maxwellian. Because relaxation problem has no direct connection to Knudsen number, this means that BGK model can be applied to high rarefied flow as long as degree of nonequilibrium is not strong in velocity distribution. Since the model-induced error in BGK depends on the degree of nonequilibirum, the BGK model is more applicable for low-speed flows than for hypersonic flows.

For engineering applications, velocity distribution function varies in the flow field and the average deviation from Maxwellian distributions may be small. In addition, the convection term also plays an important role in full BGK equation. It is unclear how model-induced error will develop in a nonlinear system, and thus how to evaluate effects of this error in a general BGK simulation is still an open question. Overall, it should be careful to apply BGK model for rarefied gas flow simulations.

Acknowledgments

We are grateful to Prof. Kun Xu for helpful discussions. This work has been supported by the National Natural Science Foundation of China (Grants No. 90816012, No. 91116013, and No. 11111120080).

Appendix: mathematic expressions integrating velocity distribution function derived with the BGK model for relaxation problems

When velocity distribution function is known, the macroscopic quantities can be integrated over the distribution function. For instance, the average of a physical quantity Q is calculated as

$$\overline{Q} = \int_{-\infty}^{\infty} Qf(u)du\,, \tag{A1}$$

and the flux of Q is

$$F(Q) = \int_{-\infty}^{\infty} Quf(u)du\,, \tag{A2}$$

or

$$F^{+}(Q) = \int_{0}^{\infty} Quf(u)du\,, \tag{A3}$$

For the BGK model, we have explicit expressions for the test problems, thus we can derive expressions for desired macroscopic quantities. Here, we give the expressions for the first moment, standard derivation, third central moment, fourth central moment, flux and half flux in x direction of mass, x-component momentum, and x-part energy for the tailored half-Maxwellian distribution case.

$$U = \overline{u} = \frac{1}{\sqrt{\pi}}\left(\frac{1}{\beta_2} - \frac{1}{\beta_1}\right), \tag{A4}$$

$$\sigma^2 = \mathrm{e}^{-t/\tau}\left[\left(\frac{1}{2}-\frac{1}{\pi}\right)\left(\frac{1}{\beta_1^2}+\frac{1}{\beta_2^2}\right)+\left(\frac{2}{\pi}-\frac{1}{2}\right)\frac{1}{\beta_1\beta_2}\right]+\left(1-\mathrm{e}^{-t/\tau}\right)\frac{1}{2\beta^2}, \tag{A5}$$

$$\int_{-\infty}^{\infty}(u-U)^3 f du = \mathrm{e}^{-t/\tau}\frac{1}{\sqrt{\pi}}\left(\frac{1}{\beta_2}-\frac{1}{\beta_1}\right)\left[\left(\frac{2}{\pi}-\frac{1}{2}\right)\left(\frac{1}{\beta_1^2}+\frac{1}{\beta_2^2}\right)-\left(\frac{4}{\pi}-\frac{3}{2}\right)\frac{1}{\beta_1\beta_2}\right], \tag{A6}$$

$$\int_{-\infty}^{\infty}(u-U)^4 f du = \frac{\mathrm{e}^{-t/\tau}}{4\pi^2}\left[\frac{48-4\pi-3\pi^2}{\beta_1\beta_2}\left(\frac{1}{\beta_1^2}+\frac{1}{\beta_2^2}\right)+\left(3\pi^2-4\pi-12\right)\left(\frac{1}{\beta_1^4}+\frac{1}{\beta_2^4}\right)+\frac{3\pi^2+16\pi-72}{\beta_1^2\beta_2^2}\right]+\left(1-\mathrm{e}^{-t/\tau}\right)\frac{3}{4\beta^4}, \tag{A7}$$

$$\frac{F_\rho^+}{\rho} = \mathrm{e}^{-t/\tau}\frac{\beta_1}{\beta_2(\beta_1+\beta_2)\sqrt{\pi}}+\frac{1-\mathrm{e}^{-t/\tau}}{2}\left[\frac{1}{\beta\sqrt{\pi}}\mathrm{e}^{-\beta^2U^2}+U\left(1+erf(\beta U)\right)\right], \tag{A8}$$

$$\frac{F_{\rho u}^+}{\rho} = \mathrm{e}^{-t/\tau}\frac{\beta_1}{2\beta_2^2(\beta_1+\beta_2)}+\frac{1-\mathrm{e}^{-t/\tau}}{2}\left[\left(U^2+\frac{1}{2\beta^2}\right)\left(1+erf(\beta U)\right)+\frac{U}{\beta\sqrt{\pi}}\mathrm{e}^{-\beta^2U^2}\right], \tag{A9}$$

$$\frac{F_{0.5\rho u^2}^+}{\rho} = \mathrm{e}^{-t/\tau}\frac{\beta_1}{2\beta_2^3(\beta_1+\beta_2)\sqrt{\pi}}+\frac{1-\mathrm{e}^{-t/\tau}}{4}\left[\frac{1+\beta^2U^2}{\beta^3\sqrt{\pi}}\mathrm{e}^{-\beta^2U^2}+\left(\frac{3U}{2\beta^2}+U^3\right)\left(1+erf(\beta U)\right)\right], \tag{A10}$$

$$\frac{F_\rho}{\rho} = \mathrm{e}^{-t/\tau}\frac{1}{(\beta_1+\beta_2)\sqrt{\pi}}\left(\frac{\beta_1}{\beta_2}-\frac{\beta_2}{\beta_1}\right)+\left(1-\mathrm{e}^{-t/\tau}\right)U\,, \tag{A11}$$

$$\frac{F_{\rho u}}{\rho} = \frac{\mathrm{e}^{-t/\tau}}{2(\beta_1+\beta_2)}\left(\frac{\beta_1}{\beta_2^2}+\frac{\beta_2}{\beta_1^2}\right)+\left(1-\mathrm{e}^{-t/\tau}\right)\left(U^2+\frac{1}{2\beta^2}\right), \tag{A12}$$

$$\frac{F_{0.5\rho u^2}}{\rho} = \frac{\mathrm{e}^{-t/\tau}}{2(\beta_1+\beta_2)\sqrt{\pi}}\left(\frac{\beta_1}{\beta_2^3}-\frac{\beta_2}{\beta_1^3}\right)+\frac{1-\mathrm{e}^{-t/\tau}}{2}\left(\frac{3U}{2\beta^2}+U^3\right). \tag{A13}$$

References

[1] C. Cercignani, The Boltzmann Equation and Its Applications, Springer-Verlag, New York, 1988.

[2] P. L. Bhatnagar, E. P. Gross, and M. Krook, A model for collision processes in gases, I. Small amplitude processes in charged and neutral one-component systems, Phys. Rev. 94 (1954) 511.

[3] L. H. Holway, Jr., Kinetic theory of shock structure using an ellipsoidal distribution function, in Rarefied Gas Dynamics: Proceedings of the Fourth International Symposium, J. H. de Leeuw (Eds.), Academic, New York, Vol. 1, 1965, pp. 193–215.

[4] E. M. Shakhov, Generalization of the Krook kinetic relaxation equation, Fluid Dyn. 3 (1968) 95.

[5] B. Francois and P. Benoit, A BGK model for small Prandtl number in the Navier-Stokes approximation, J. Stat. Phys. 71 (1993) 191.

[6] H. Struchtrup, The BGK model with velocity dependent collision frequency, Continuum Mech. Thermodyn. 9 (1997) 23.

[7] R. C. K. Leung, E. W. S. Kam, and R. M. C. So, Recovery of transport coefficients in Navier-Stokes equations from modeled Boltzmann equation, AIAA J. 45 (2007) 737.

[8] A. Aimi, M. Diligenti, M. Groppi, and C. Guardasoni, On the numerical solution of a BGK-type model for chemical reactions, Eur. J. Mech. B 26 (2007) 455.

[9] J. Kerimo and S. S. Girimaji, Boltzmann-BGK approach to simulating weakly compressible 3D turbulence: comparison between lattice Boltzmann and gas kinetic methods, J. Turb. 8 (2007) N46.

[10] Z.-H. Li and H.-X. Zhang, Gas-kinetic numerical studies of three-dimensional complex flows on spacecraft re-entry, J. Compu. Phys. 228 (2009) 1115.

[11] M. A. Gallis and J. R. Torczynski, Investigation of the ellipsoidal-statistical Bhatnagar-Gross-Krook kinetic model applied to gas-phase transport of heat and tangential momentum between parallel walls, Phys. Fluids 23 (2011) 030601.

[12] R. Kumar, E. V. Titov, D. A. Levin, N. E. Gimelshein, and S. F. Gimelshein, Assessment of Bhatnagar-Gross-Krook approaches for near continuum regime nozzle flows, AIAA J. 48 (2010) 1531.

[13] P. Andries, K. Aoki, and B. Perthame, A consistent BGK-type model for gas mixtures, J. Stat. Phys. 106 (2002) 993.

[14] L. Mieussens and H. Struchtrup, Numerical comparison of BGK-models with proper Prandtl number, Phys. Fluids 16 (2004) 2797.

[15] K. Xu and J. C. Huang, A unified gas-kinetic scheme for continuum and rarefied flows, J. Comput. Phys. 229 (2010) 7747.

[16] J. C. Huang, K. Xu, and P. Yu, A unified gas-kinetic scheme for continuum and rarefied flows III : Microflow simulations, Comm. Comput. Phys. (in press).

[17] W. G. Vincenti and C. H. Kruger, Introduction to Physical Gas Dynamics, John Wiley & Sons, New York, 1965.

[18] G. A. Bird, Molecular Gas Dynamics and the Direct Simulation of Gas Flows, Clarendon Press, Oxford, 1994.

[19] K. Xu, A gas-kinetic BGK scheme for the Navier–Stokes equations and its connection with artificial dissipation and Godunov method, J. Comput. Phys. 171 (2001) 289.

[20] W. Wagner, A convergence proof for Bird's direct simulation Monte Carlo method for the Boltzmann equation, J. Stat. Phys. 66 (1992) 1011.

[21] D. J. Rader, M. A. Gallis, J. R. Torczynski, and W. Wagner, Direct Simulation Monte Carlo convergence behavior of the hard-sphere-gas thermal conductivity for Fourier heat flow, Phys. Fluids 18 (2006) 077102.

[22] Q. Sun and I. D. Boyd, Evaluation of macroscopic properties in the direct simulation Monte Carlo method, J. Thermophys. Heat Transf. 19 (2005) 329.

[23] C. Cai and C. Zhou, Planar collisionless jet impingement on a specular reflective plate, Theor. Appl. Mech. Lett. 2 (2012) 022001.